PCCP

PAPER

View Article Online
View Journal | View Issue

Cite this: *Phys. Chem. Chem. Phys.*, 2016, **18**, 5397

In situ characterization of the decomposition behavior of $Mg(BH_4)_2$ by X-ray Raman scattering spectroscopy

Christoph J. Sahle,*[ab] Simon Kujawski,[c] Arndt Remhof,[d] Yigang Yan,[d] Nicholas P. Stadie,[d] Ali Al-Zein,[a] Metin Tolan,[c] Simo Huotari,[b] Michael Krisch[a] and Christian Sternemann[c]

Received 28th October 2015,
Accepted 24th December 2015

DOI: 10.1039/c5cp06571b

www.rsc.org/pccp

We present an *in situ* study of the thermal decomposition of $Mg(BH_4)_2$ in a hydrogen atmosphere of up to 4 bar and up to 500 °C using X-ray Raman scattering spectroscopy at the boron K-edge and the magnesium $L_{2,3}$-edges. The combination of the fingerprinting analysis of both edges yields detailed quantitative information on the reaction products during decomposition, an issue of crucial importance in determining whether $Mg(BH_4)_2$ can be used as a next-generation hydrogen storage material. This work reveals the formation of reaction intermediate(s) at 300 °C, accompanied by a significant hydrogen release without the occurrence of stable boron compounds such as amorphous boron or $MgB_{12}H_{12}$. At temperatures between 300 °C and 400 °C, further hydrogen release proceeds *via* the formation of higher boranes and crystalline MgH_2. Above 400 °C, decomposition into the constituting elements takes place. Therefore, at moderate temperatures, $Mg(BH_4)_2$ is shown to be a promising high-density hydrogen storage material with great potential for reversible energy storage applications.

1 Introduction

Zero-emission propulsion is a long standing societal goal that would contribute to restricting the consumption of fossil fuels and limiting the extent of anthropogenically caused climate change.[1,2] Besides energy storage in electrochemical cells, storage of hydrogen as an energy carrier is a promising step toward realizing this dream. However, hydrogen storage, especially for mobile applications, remains challenging.[3] Conventional strategies, *i.e.* liquefying or pressurizing hydrogen, present the challenges that the resulting storage devices are large and heavy, and therefore do not meet the targets set *e.g.* by the Department of Energy.[4]

Promising alternatives for hydrogen storage include liquid organic hydrogen carriers,[5] metal organic frameworks,[6] carbon nanostructures,[7–9] and metal borohydrides.[10] Hydrogen storage in the solid state, especially in metal borohydrides, is desirable, since these materials can offer simultaneous high gravimetric and volumetric hydrogen densities.[11] For metal borohydrides – such as $LiBH_4$, $NaBH_4$, $Mg(BH_4)_2$, and $Ca(BH_4)_2$ – to function as hydrogen storage materials, reversible desorption, *i.e.* cyclability, is necessary. However, the reversibility of the decomposition reactions of borohydrides can be hindered by unwanted reaction intermediates, such as for example the $[B_{12}H_{12}]^{2-}$-phases in $LiBH_4$ and $NaBH_4$. These phases are kinetically stable and thus hinder the reversibility.[11] Although it was found that decomposition proceeds in multiple steps and is even partially reversible, the details of the decomposition mechanisms and possible formation of stable boron phases in the intermediate steps is still debated. The amorphous nature of some of the final and intermediate compounds makes the investigation of the important details of the de- and re-hydrogenation mechanisms difficult. Furthermore, these details strongly depend on the experimental conditions and thus need to be investigated *in situ*.

$Mg(BH_4)_2$ is one of the most promising metal borohydride hydrogen storage materials due to its moderate enthalpy of decomposition and has been studied widely in the recent years.[12–18] Hydrogen desorption was investigated with a particular focus on the possible formation of closoboranes under different thermal conditions and in different gaseous media such as hydrogen, argon, and helium or under dynamic vacuum conditions resulting in a variety of suggested decomposition pathways.[15,19–23] The formation of $MgB_{12}H_{12}$, even in the early stages of decomposition, is often inferred by solid-state-nuclear magnetic resonance (NMR) or evidenced indirectly *via* solution NMR.

[a] *ESRF-The European Synchrotron, Grenoble Cedex 9, France. E-mail: christoph.sahle@esrf.fr*
[b] *Department of Physics, University of Helsinki, POB 64, FI-00014, Helsinki, Finland*
[c] *Fakultät Physik/DELTA, Technische Universität Dortmund, Dortmund, Germany. E-mail: christian.sternemann@tu-dortmund.de*
[d] *Materials for Energy Conversion, Empa, Ch-8600 Dübendorf, Switzerland*

The presence of $[B_{12}H_{12}]^{2-}$ would not support the use of $Mg(BH_4)_2$ for applications in cycleable hydrogen storage devices due to the kinetically unfavorable re-hydrogenation. Hence, full decomposition into MgB_2 is necessary for cycling,[15] which calls for reaction conditions with temperatures that are not suited for portable storage media. However, it was recently shown that $Mg(BH_4)_2$ decomposes under dynamic vacuum conditions up to 400 °C without the formation of $MgB_{12}H_{12}$.[23] Here, $[B_{12}H_{12}]^{2-}$ was observed as a part of the polymeric intermediate MgB_xH_y between 265 °C and 300 °C, which first converts into amorphous B, Mg, and MgH_2 at 400 °C and then converts completely into MgB_2 at 500 °C.[23] Other reports proposed a gradual B–H condensation process from $[BH_4]^-$ to higher boranes in the decomposition of $Mg(BH_4)_2$.[15,24] Furthermore, there are also studies suggesting the formation of $MgB_{12}H_{12}$ species during the dehydrogenation.[19,20] However, the reaction conditions and, especially, the gaseous atmospheres under which those various investigations took place were not the same and, importantly, may not be applicable to practical applications. To improve reversibility and possibly modify the reaction pathways, these must be understood. Different borohydrides decompose along different pathways without a general rule. For some compounds there seems to be an emerging agreement, but the hydrogen release reactions of $Mg(BH_4)_2$ are still under discussion. So far, there are only a few inconclusive *in situ* X-ray diffraction (XRD)[18,25,26] and infrared spectroscopy studies[26] reported in the literature and a dependence on the presence of impurities remains an open question.[18,25] Hence, experimental *in situ* studies using complementary methods are highly desireable. We apply X-ray Raman scattering (XRS) spectroscopy at both, the boron K- and magnesium $L_{2,3}$-core levels, to analyze the *in situ* decomposition of $Mg(BH_4)_2$ under hydrogen atmosphere (up to 4 bar) at temperatures up to 500 °C. XRS provides the unique and powerful capability to investigate these amorphous and/or nanocrystalline products *in situ* and under well-defined thermodynamic conditions. We find that after the transition from the low temperature α/γ-$Mg(BH_4)_2$ phase to the high temperature β-phase, significant amounts of intermediate compound(s) form, which, at higher temperatures, decompose into mostly B, MgH_2, and Mg. We quantify the amount of different phases present during the decomposition and discuss possible strategies to identify the intermediate phase(s) that occur(s) at lower temperatures.

2 Experimental

XRS combines the benefits of soft-X-ray spectroscopy and the properties of hard X-rays making it a valuable method for the *in situ* study of lightweight/low-Z hydrogen storage materials.[27] For example, this non-resonant inelastic X-ray scattering technique has already been used to study the B K-edge in MgB_2, BN, $C_2B_{10}H_{12}$, B_2O_3, and $Li_2B_4O_7$.[28–32] Likewise, the Mg $L_{2,3}$-edges of, for example, elemental Mg have also been studied.[33,34] The use of hard X-rays as a probe allows the *in situ* study of low-atomic-weight bulk samples under various reaction atmospheres and even at extreme conditions.[35–37] Recently, Miedema *et al.* have demonstrated the capabilities of *in situ* XRS spectroscopy to investigate hydrogen desorption in the possible hydrogen storage materials $LiBH_4$ and $LiBH_4/NaBH_4$ nanocomposites.[38,39]

In this work, XRS spectra were collected at beamline ID20 of the European Synchrotron Radiation Facility. The beam size on the sample was 150 μm × 250 μm (V × H). The spectrometer employed 36 Si(660) analyzer crystals with a mean scattering angle of 50° (used in the case of the B K-edge), and 24 analyzers with a mean scattering angle of 120° (for the Mg $L_{2,3}$-edges). This results in momentum transfers of 4.2 ± 0.5 $Å^{-1}$ (probing mostly p-DOS) and 8.5 ± 0.5 $Å^{-1}$ (probing a mixture of s-, p-, and d-DOS), respectively. The choice of these different momentum transfers for the two different edges is dictated by the energy-loss position of the dominating Compton profile, which varies as a function of momentum transfer. The core onset extraction from the data is feasible if the peak of the Compton profile is far enough from the energy region of interest; hence in XRS different edges must often be measured with different momentum transfers. The overall energy resolution was 0.6 eV.

We purchased $Mg(BH_4)_2$ and all reference materials, *i.e.* amorphous B, H_3BO_3, MgB_2, MgH_2, and MgO, from Sigma-Aldrich and used them without further processing except for the nanoscale $MgB_{12}H_{12}$/carbon sample, which we prepared by a gas–solid reaction of carbon-supported $Mg(BH_4)_2$ with a B_2H_6/H_2 atmosphere, as previously discussed.[40]

We used a custom high-temperature/high-pressure sample cell for the *in situ* measurements, as described in detail elsewhere.[41] In short, we pressed the native $Mg(BH_4)_2$ powder into a circular, resistively heated sample holder (see inset in Fig. 1(b)) and covered the sample using Be foil (0.1 mm thickness) to prevent sample spillage during annealing. The reaction chamber was closed by a half-spherical Be dome (wall thickness 1.7 mm), which allowed a field of view of 2π for the incident and scattered X-rays. With this cell, we performed measurements at ambient conditions (room temperature/pressure) as well as at temperatures between 200 °C and 500 °C in steps of 100 °C. At each temperature, we measured several XRS spectra first of the of B K-edge and then the Mg $L_{2,3}$-edge, checked them for consistency, and averaged signals from several analyzer crystals and different scans. Only the spectra of the boron K-edge measured at 300 °C exhibited a slight time dependence, which we will discuss later. The desired core edges were extracted from the overall spectrum by removing the contribution from valence electrons using parameterized PearsonVII functions. Details of the data analysis can be found elsewhere.[42,43] We normalized all XRS curves to the area below the spectra in the energy loss range from 185–212 eV (45–65 eV) for the B (Mg) edge. In this way, the dependence on the stoichiometry of the sample is not considered; *i.e.*, $MgB_{12}H_{12}$ has 12 B atoms per formula unit whereas H_3BO_3 only has one B atom per formula unit, and the fit parameters describe the contribution of a single B atom within each compound to the scattering signal. However, since the formula units are known, the stoichiometries can simply be derived, as shown in parentheses in Table 1 alongside the fit parameters. For Mg, the stoichiometric- and

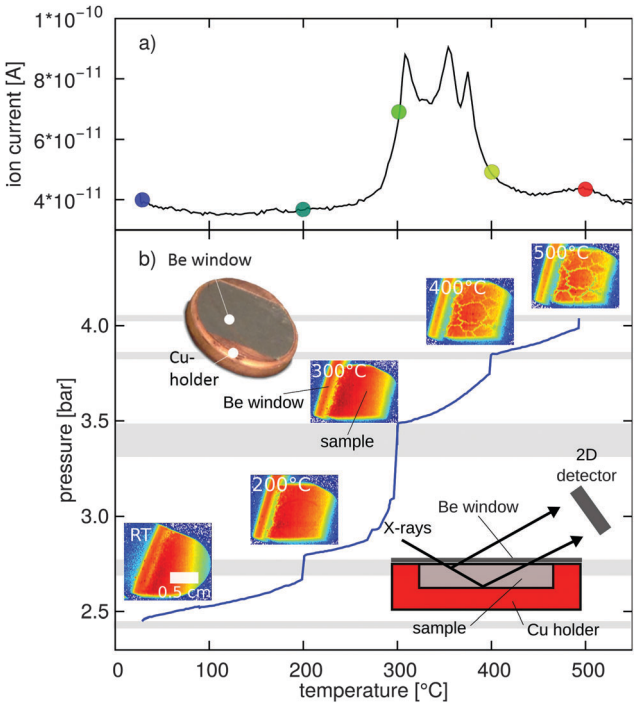

Fig. 1 (a) Hydrogen evolution measured at a constant heating rate of 10 °C min^{-1} using mass spectrometry (MS) for comparison to *in situ* XRS data. The colored dots indicate the temperatures chosen for XRS spectra. (b) *In situ* measurement of gas pressure inside the sample chamber as a function of temperature measured during XRS experiments. The gray shaded areas indicate the regions corresponding to each XRS spectrum. The insets pictures are (top left) the exposed Cu sample holder filled with $Mg(BH_4)_2$ and covered with a Be window, (along the *p*–*T*-curve) tomography images collected just before the *in situ* XRS measurements at the respective temperatures, and (bottom right) a schematic drawing of a vertical cut through the sample holder and its orientation with respect to incoming X-rays and the detector.

fit-values are equivalent since each compound only has one Mg atom per formula unit.

3 Results and discussion

Fig. 1(a) shows the temperature dependent H_2 evolution of $Mg(BH_4)_2$ measured by mass spectrometry at a constant heating rate of 10 °C min^{-1}, which was used to find optimized annealing temperatures for the XRS measurement. We chose to measure *in situ* XRS spectra at the temperatures indicated by colored dots in the image: at 200 °C, before decomposition, at 300 °C to investigate possible intermediate reaction compounds at the initial stage of hydrogen release, and at 400 °C and 500 °C to investigate the solid products remaining after hydrogen release.

The approximately corresponding pressure–temperature relation measured during the *in situ* XRS experiment is shown in Fig. 1(b). In this case, the sample was heated to the indicated temperature and we waited until the vapor pressure reached an approximate equilibrium. The *p*–*T*-regimes during which we recorded XRS spectra are indicated by gray shaded areas in Fig. 1. The pressure increase during heating is a combined effect from both, gas law expansion and H_2 release from $Mg(BH_4)_2$. During the measurements at above-ambient temperature, we observed continued hydrogen desorption and thus expect further decomposition on much longer time scales. Hence, the measured spectra depict an averaged snapshot of the sample composition in a non-equilibrium state on a timescale of 2 hours rather than the final reaction products at a certain temperature. At each temperature, directly before the XRS measurement, we collected tomographic images of the sample (the details of this technique are reported elsewhere[44]), shown as insets in Fig. 1(b). In the last steps of decomposition, we observed macroscopic cracks in the sample (just before 400 °C and at 500 °C). At these temperatures, the sample pellet's integrity is likely to be compromised due to large volume changes during the formation of Mg and MgO, as discussed later, as well as possible heat and gas evolution.

Fig. 2 shows the *in situ* spectra of the B K-edge and the Mg $L_{2,3}$-edges. The minor differences between the spectra at room temperature and at 200 °C are due to the structural phase transition of α/γ-$Mg(BH_4)_2$ to β-$Mg(BH_4)_2$, which occurs between 180 °C and 190 °C.[13,45,46] There is an associated small release of H_2 already at 200 °C, which may be due to the presence of impurities.[18] At temperatures above 200 °C, β-$Mg(BH_4)_2$ starts to decompose, which is manifested by more dramatic changes in both the B K-edge and the Mg $L_{2,3}$-edges (prominent changes are marked by arrows in Fig. 2(a) and (b)).

The *in situ* XRS spectra can be compared to XRS spectra of reference compounds measured at room temperature to analyze the dehydrogenation reaction pathway of $Mg(BH_4)_2$. Here, we use a multi-component analysis method to quantify the phases present at each stage during thermal decomposition. We considered various prominent candidates for decomposition and intermediate products: B, a $MgB_{12}H_{12}$/carbon compound, MgB_2, and metallic Mg, as well as H_3BO_3 and MgO to detect possible sample oxidation. These reference spectra are shown in Fig. 2(c) and (d). The XRS spectrum of metallic Mg was previously reported[34] and all other spectra were measured in this work. The presence of numerous unique features in each reference spectrum allow each to be used as fingerprints to identify the

Table 1 Fit parameters and molar fractions (in parentheses) from multi-component analysis of the B K-edge. Dashes (—) indicate that this compound was neglected in the fit. The asterisk indicates that these values are in favor of an occurrence of an intermediate instead of $MgB_{12}H_{12}$ and B as discussed in the text

T [°C]	$MgB_{12}H_{12}$	B	β-$Mg(BH_4)_2$
300	0.12 ± 0.02 (0.02 ± 0.05)*	0.23 ± 0.02 (0.41 ± 0.06)*	0.64 ± 0.02 (0.57 ± 0.05)
400	0.95 ± 0.02 (0.61 ± 0.08)	0.05 ± 0.02 (0.39 ± 0.14)	—
500	0.71 ± 0.08 (0.17 ± 0.04)	0.29 ± 0.04 (0.83 ± 0.10)	—

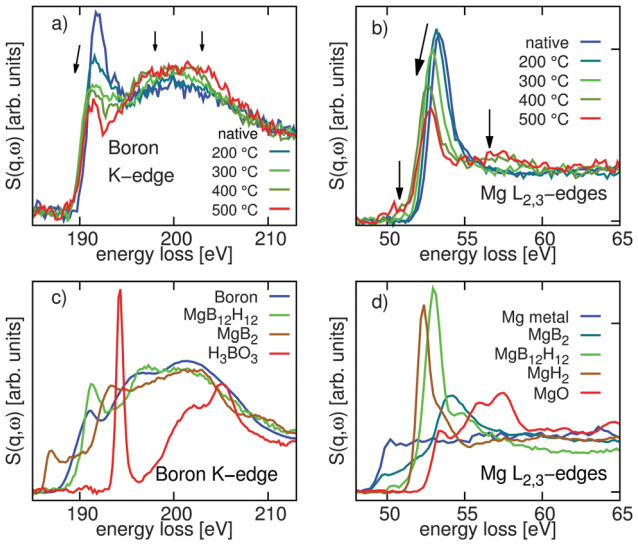

Fig. 2 XRS spectra of $Mg(BH_4)_2$ at the (a) B K-edge and (b) Mg $L_{2,3}$-edges, measured during thermal decomposition. (c) XRS spectra at the B K-edge of various B-containing reference compounds at room temperature. (d) XRS spectra at the Mg $L_{2,3}$-edges of various Mg-containing reference compounds at room temperature.

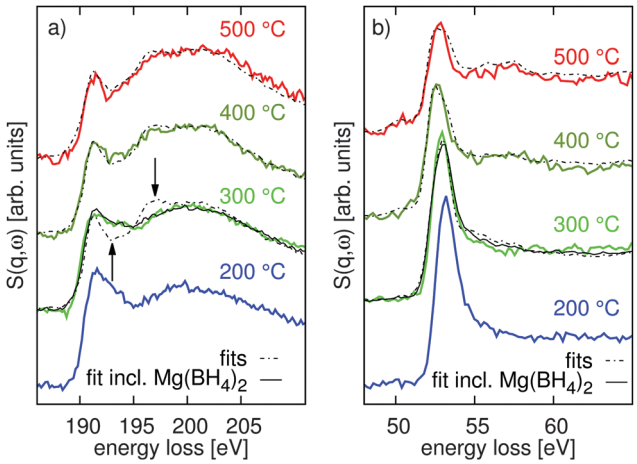

Fig. 3 XRS spectra of $Mg(BH_4)_2$ at the (a) B K-edge and (b) Mg $L_{2,3}$-edges at different temperatures during thermal decomposition; experimental results (colored lines) and multi-component fits (black dashed and solid lines). The spectra are plotted with vertically offset for clarity.

main decomposition products of native $Mg(BH_4)_2$ by a multi-component fitting method. The $MgB_{12}H_{12}$/carbon-reference is representative of a wide variety of higher Mg boranes ($Mg_xB_yH_z$) with a similar local chemical environment of B and Mg.

The multi-component fit of the B K-edge was performed by considering contributions from B and $MgB_{12}H_{12}$, except for the initial decomposition at 300 °C where, in addition, we also considered the β-$Mg(BH_4)_2$ phase (spectrum measured at 200 °C). Occurence of β-$Mg(BH_4)_2$ for higher temperatures and occurence of MgB_2 in the whole temperature range could be excluded due to the analysis of the Mg L-edge as discussed later. The possibility of the oxidation of boron during annealing was excluded due to the lack of any feature at 194 eV (compare *e.g.* Miedema *et al.*[38]) and hence H_3BO_3 was not a component in the fit. The Mg $L_{2,3}$-edges were fitted with contributions from all six Mg-containing references: $MgB_{12}H_{12}$, metallic Mg, MgH_2, MgB_2, MgO, and the β-$Mg(BH_4)_2$ phase. The best fit results are shown in Fig. 3 and the resulting best fit parameters are given in Tables 1 and 2.

B K-edge

A representative fit of the B K-edge at 300 °C could be achieved only when β-$Mg(BH_4)_2$ is considered as a reference for this temperature as well. Analyzing the time dependence of the B K-edge spectra taken at 300 °C we find a decreasing amount of this phase with annealing on timescales below 1 h. The amount of $MgB_{12}H_{12}$ and B estimated from this fit at 300 °C is far from resembling the stoichiometry of the starting material, indicating that none of theses compounds is a major constituent of the sample a this temperature. We conclude that after transition to the high-temperature phase of $Mg(BH_4)_2$ at 200 °C, the sample starts to decompose when heated to 300 °C and hydrogen gas is released. This implies the absence of both $MgB_{12}H_{12}$ and solid B in the decomposition product, and points to the formation of an unknown intermediate phase. This intermediate phase has been identified as $Mg(B_3H_8)_2$ in other work.[23,24]

We find a good agreement between the measured spectrum at 400 °C and a fit involving our $MgB_{12}H_{12}$ reference sample and small amounts of B. At 500 °C, the spectral weight of B increases significantly at the expense of the $MgB_{12}H_{12}$ contribution, suggesting that some of the $MgB_{12}H_{12}$-like phase decomposes into elemental B and Mg during the observed H_2 release. $MgB_{12}H_{12}$ has been found to decompose at temperatures above 400 °C into B and Mg.[40] At all temperatures explored in this work, the occurrence of MgB_2 could be ruled out due to its prominent pre-edge feature at 187 eV. This is in contrast to earlier studies employing vacuum conditions.[14,23] We note that the present results characterize the non-equilibrium composition of the sample upon annealing for times on the order of 2 h and might not describe the final composition after long-term annealing at the same temperatures. Consequently, the results obtained here should be used to identify decomposition reaction pathways including amorphous reaction products, but not necessarily to identify equilibrium states.

The $MgB_{12}H_{12}$ carbon-nanocomposite reference material, has been used in this work to identify contributions from $MgB_{12}H_{12}$-like species, including $MgB_{12}H_{12}$ (as suggested in other work[15]), $B_{12}H_{12}$ dimers, or larger borane polymers interconnected by Mg atoms as they may show similar Mg and B fingerprints due to their similar chemical environment.[40] However, assuming $MgB_{12}H_{12}$ to be a decomposition product according to the fit of the B K-edge at 400 °C and 500 °C, results in a larger Mg : B ratio than expected from the 1 : 2 stoichiometry of the starting material which will be discussed after evaluation of the Mg L-edges.

Mg $L_{2,3}$-edges

The high-temperature phase of $Mg(BH_4)_2$ decomposes upon annealing at 300 °C. The corresponding fit gives similar

Table 2 Fit parameters (*i.e* molar fractions) from multi-component analysis of the Mg $L_{2,3}$-edge. The asterisk indicates values that favor the occurrence of an intermediate rather than $MgB_{12}H_{12}$ as discussed in the text

T [°C]	$MgB_{12}H_{12}$	MgH_2	Metallic Mg	MgO	β-$Mg(BH_4)_2$
300	(0.32 ± 0.05)*	0.28 ± 0.05	0.01 + 0.04	0.00 + 0.04	0.35 ± 0.02
400	0.29 ± 0.05	0.50 ± 0.01	0.15 ± 0.03	0.16 ± 0.04	0.00 + 0.04
500	0.23 ± 0.05	0.35 ± 0.02	0.21 ± 0.01	0.27 ± 0.02	0.00 + 0.04

contributions of MgH_2 and β-$Mg(BH_4)_2$. Although we find signatures of our $MgB_{12}H_{12}$ reference spectrum in the *in situ* data at 300 °C, the occurrence of $MgB_{12}H_{12}$ can be ruled out at this temperature based on the B K-edge analysis. Also, the mismatch of $MgB_{12}H_{12}$: $Mg(BH_4)_2$ ratios extracted from both edges independently may be due to the proceeding decomposition of $Mg(BH_4)_2$ during the measurements at 300 °C. This finding is consistent with the presence of an unknown intermediate phase and the formation of MgH_2.

This intermediate phase then decomposes into a $MgB_{12}H_{12}$-like phase (as discussed above), MgH_2, metallic Mg, and small amounts of B (as inferred from the B K-edge fit) between 300 °C and 400 °C. In addition, a contribution from MgO was observed at high temperatures as indicated by the spectral feature at 57 eV energy loss. Most probably, part of the metallic Mg decomposition product was oxidized by residual oxygen in the reaction chamber. Elemental Mg is clearly present in the sample at this temperature because of the small pre-edge shoulder at around 51 eV in the Mg $L_{2,3}$-edges. Between 400 °C and 500 °C, the spectral weights of $MgB_{12}H_{12}$ and MgH_2 decrease, whereas those of metallic Mg and – correspondingly – of MgO increase. We infer from this that $MgB_{12}H_{12}$-like species as well as MgH_2 decompose into elemental Mg and B accompanied by hydrogen release (also reported elsewhere[40]). The increasing contribution of Mg is coupled to an increase in MgO content. The decrease of $MgB_{12}H_{12}$ and MgH_2 content directly converts to an increase of Mg and MgO content within the errors of the fit. Deviations of the fits from the measured spectra may be due to the fact that we used a nanocomposite $MgB_{12}H_{12}$ sample as a reference. Comparing the fit results obtained for the Mg $L_{2,3}$- and B K-edges, similar amounts of decomposed $MgB_{12}H_{12}$ (or $MgB_{12}H_{12}$-like phases) are found. It should be noted, that at 500 °C contributions from $MgB_{12}H_{12}$-like species and MgH_2 are still present in the sample, suggesting that the decomposition reaction is slow and not fully completed. Furthermore, the stoichiometric analysis of all Mg- and B-containing phases based on the fits of both edges yields an Mg : B ratio of approximately 1 : 4 if $MgB_{12}H_{12}$ is assumed to be the decomposition product. This ratio deviates significantly from the 1 : 2 ratio of the native $Mg(BH_4)_2$, which implies that instead of $MgB_{12}H_{12}$, a polymer or other intermediate is present with a stoichiometry of 1 : 6 (Mg : B) that exhibits a similar local Mg and B environment compared to $MgB_{12}H_{12}$.

Decomposition pathway

The information obtained in this work from both the B K-edge and the Mg $L_{2,3}$-edges gives a detailed picture of the thermal decomposition of $Mg(BH_4)_2$. It must be emphasized that in this current case, the results obtained give *in situ* snapshots of the sample during the decomposition process rather than information about equilibrium states. The high temperature phase of $Mg(BH_4)_2$ decomposes into MgH_2 and an intermediate phase or a mixture of intermediates which cannot be further identified at 300 °C. This phase then transforms at 400 °C into MgH_2, Mg, and elemental B, either *via* the formation of $MgB_{12}H_{12}$-like species with smaller Mg to B ratio and subsequent decomposition or *via* a polymerization process as described in other work.[23,24] At 500 °C MgH_2 decomposes into elemental Mg. All phases of the decomposition are accompanied by the release of hydrogen gas (Fig. 4).

The present study shows that the intermediate formed in the main decomposition step of $Mg(BH_4)_2$ (between 200 °C and 300 °C) is not $MgB_{12}H_{12}$ and supports earlier studies,[23] namely that an intermediate with $Mg_xB_yH_z$ stoichiometry forms first, together with MgH_2. This intermediate might be $Mg(B_3H_8)_2$ as identified in these earlier studies[23,24] which would be consistent with the estimated stoichiometry using our fit results. At higher temperatures, MgH_2 decomposes into Mg and H_2, while the intermediate $Mg_xB_yH_z$ may react under the release of hydrogen to growing agglomerates containing $B_{12}H_{12}$-like units until, finally, all hydrogen is released. Between 300 °C and

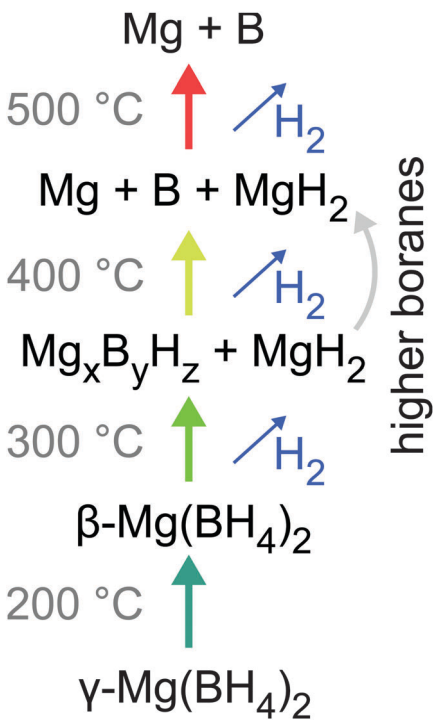

Fig. 4 Schematic summary of the thermal decomposition of $Mg(BH_4)_2$.

400 °C a significant amount of hydrogen release can be achieved without the occurrence of unwanted byproducts such as $MgB_{12}H_{12}$ and elemental B. It is unknown from this work whether the reaction, if stopped at 300 °C, would proceed further given more time.

In order to identify the intermediate products in the early stages of the decomposition by XRS, it would be desirable to measure the reference spectra of possible intermediate products discussed elsewhere in the literature (*e.g.* ref. 47 and 48) and incorporate them into the multi-component fitting analysis. However, many of these possible intermediate structures were predicted *via* theoretical modeling and are difficult to synthesize or are unstable in freestanding form. Nevertheless, experimental XRS spectra may provide a unique benchmark for calculated XRS spectra both at the Mg $L_{2,3}$- and B K-edges of the proposed intermediates.

4 Summary and outlook

We have presented an *in situ* XRS spectroscopy study of the thermal decomposition of $Mg(BH_4)_2$ to understand the reaction pathway during hydrogen desorption. From the XRS spectra we could infer quantitative information even on amorphous products during the decomposition of borohydrides. Our work opens new perspectives for future investigations, *e.g.* of nano-confined samples, layer-protected hydrides, and eutectic mixtures. Spectral fingerprinting *via* multi-component fits of measured reference compounds to the *in situ* spectra of the decomposing $Mg(BH_4)_2$ were used to identify the major decomposition products. Consistent information from the B K-edge and the Mg $L_{2,3}$-edges suggests the formation of yet to be identified intermediate decomposition products at temperatures up to 300 °C and the subsequent decomposition of these intermediates into a phase with an Mg : B stoichometry of 1 : 6 and $MgB_{12}H_{12}$-like spectral shape as well as MgH_2 and elemental B at 400 °C. Further annealing yields mainly B and Mg. XRS has proven to be a valuable tool to infer quantitative information on even amorphous products during the decomposition reaction and opens new possibilities for future investigations. Future theoretical approaches may yield information about the intermediate compounds. During the decomposition of $Mg(BH_4)_2$ at 300 °C, we observe a significant release of hydrogen gas without the formation of stable B phases, which highlights the great promise of $Mg(BH_4)_2$ as a reversible hydrogen storage medium.

Acknowledgements

We acknowledge Harald Müller and Christian Henriquet for expert help and assistance during the experiment. We thank the European Synchrotron Radiation Facility for providing synchrotron radiation and the technical and scientific staff of the ESRF beamline ID20 for support and valuable discussions. This work was supported by the Academy of Finland (Grants 1254065, 1283136, and 1259526) and the University of Helsinki Research Funds (Grants 490076 and 490064). Y. Yan and A. Remhof would like to acknowledge the financial support granted by Switzerland through the Swiss contribution to the enlarged European Union.

References

1 A. J. Churchard, E. Banach, A. Borgschulte, R. Caputo, J.-C. Chen, D. Clary, K. J. Fijalkowski, H. Geerlings, R. V. Genova and W. Grochala, *et al.*, *Phys. Chem. Chem. Phys.*, 2011, **13**, 16955–16972.
2 C. Liu, F. Li, L.-P. Ma and H.-M. Cheng, *Adv. Mater.*, 2010, **22**, E28–E62.
3 L. Schlapbach and A. Züttel, *Nature*, 2001, **414**, 353–358.
4 DOE Targets for Onboard Hydrogen Storage Systems for Light-Duty Vehicles.
5 D. Teichmann, W. Arlt, P. Wasserscheid and R. Freymann, *Energy Environ. Sci.*, 2011, **4**, 2767–2773.
6 N. L. Rosi, J. Eckert, M. Eddaoudi, D. T. Vodak, J. Kim, M. O'Keeffe and O. M. Yaghi, *Science*, 2003, **300**, 1127–1129.
7 B. Panella, M. Hirscher and S. Roth, *Carbon*, 2005, **43**, 2209–2214.
8 Z. Yang, Y. Xia and R. Mokaya, *J. Am. Chem. Soc.*, 2007, **129**, 1673–1679.
9 N. P. Stadie, J. J. Vajo, R. W. Cumberland, A. A. Wilson, C. C. Ahn and B. Fultz, *Langmuir*, 2012, **28**, 10057–10063.
10 S.-i. Orimo, Y. Nakamori, J. R. Eliseo, A. Züttel and C. M. Jensen, *Chem. Rev.*, 2007, **107**, 4111–4132.
11 H.-W. Li, Y. Yan, S.-i. Orimo, A. Züttel and C. M. Jensen, *Energies*, 2011, **4**, 185–214.
12 R. Černý, Y. Filinchuk, H. Hagemann and K. Yvon, *Angew. Chem.*, 2007, **119**, 5867–5869.
13 J.-H. Her, P. W. Stephens, Y. Gao, G. L. Soloveichik, J. Rijssenbeek, M. Andrus and J.-C. Zhao, *Acta Crystallogr., Sect. B: Struct. Sci.*, 2007, **63**, 561–568.
14 N. Hanada, K. Chłopek, C. Frommen, W. Lohstroh and M. Fichtner, *J. Mater. Chem.*, 2008, **18**, 2611–2614.
15 G. L. Soloveichik, Y. Gao, J. Rijssenbeek, M. Andrus, S. Kniajanski, R. C. Bowman, S.-J. Hwang and J.-C. Zhao, *Int. J. Hydrogen Energy*, 2009, **34**, 916–928.
16 Y. Yan, Y. S. Au, D. Rentsch, A. Remhof, P. E. de Jongh and A. Züttel, *J. Mater. Chem. A*, 2013, **1**, 11177–11183.
17 Y. S. Au, Y. Yan, K. P. De Jong, A. Remhof and P. E. De Jongh, *J. Phys. Chem. C*, 2014, **118**, 20832–20839.
18 N. P. Stadie, E. Callini, B. Richter, T. R. Jensen, A. Borgschulte and A. Züttel, *J. Am. Chem. Soc.*, 2014, **136**, 8181–8184.
19 S.-J. Hwang, R. C. Bowman, J. W. Reiter, J. Rijssenbeek, G. L. Soloveichik, J.-C. Zhao, H. Kabbour and C. C. Ahn, *J. Phys. Chem. C*, 2008, **112**, 3164–3169.
20 H. Li, K. Miwa, N. Ohba, T. Fujita, T. Sato, Y. Yan, S. Towata, M. Chen and S. Orimo, *Nanotechnology*, 2009, **20**, 204013.
21 G. Severa, E. Rönnebro and C. M. Jensen, *Chem. Commun.*, 2010, **46**, 421–423.
22 S. Gupta, I. Z. Hlova, T. Kobayashi, R. V. Denys, F. Chen, I. Y. Zavaliy, M. Pruski and V. K. Pecharsky, *Chem. Commun.*, 2013, **49**, 828–830.

23 Y. Yan, A. Remhof, D. Rentsch and A. Züttel, *Chem. Commun.*, 2015, **51**, 700–702.
24 M. Chong, A. Karkamkar, T. Autrey, S.-i. Orimo, S. Jalisatgi and C. M. Jensen, *Chem. Commun.*, 2011, **47**, 1330–1332.
25 K. Chłopek, C. Frommen, A. Léon, O. Zabara and M. Fichtner, *J. Mater. Chem.*, 2007, **17**, 3496–3503.
26 M. Paskevicius, M. B. Ley, D. A. Sheppard, T. R. Jensen and C. E. Buckley, *Phys. Chem. Chem. Phys.*, 2013, **15**, 19774–19789.
27 W. Schülke, *Electron dynamics by inelastic X-ray scattering*, OUP Oxford, 2007.
28 A. Mattila, J. Soininen, S. Galambosi, S. Huotari, G. Vankó, N. Zhigadlo, J. Karpinski and K. Hämäläinen, *Phys. Rev. Lett.*, 2005, **94**, 247003.
29 S. K. Lee, P. J. Eng, H.-k. Mao, Y. Meng, M. Newville, M. Y. Hu and J. Shu, *Nat. Mater.*, 2005, **4**, 851–854.
30 S. K. Lee, P. J. Eng, H.-k. Mao, Y. Meng and J. Shu, *Phys. Rev. Lett.*, 2007, **98**, 105502.
31 Y. Feng, J. Soininen, A. Ankudinov, J. Cross, G. Seidler, A. Macrander, J. Rehr and E. Shirley, *Phys. Rev. B: Condens. Matter Mater. Phys.*, 2008, **77**, 165202.
32 T. T. Fister, F. D. Vila, G. T. Seidler, L. Svec, J. C. Linehan and J. O. Cross, *J. Am. Chem. Soc.*, 2008, **130**, 925–932.
33 T. Fister, G. Seidler, L. Wharton, A. Battle, T. Ellis, J. Cross, A. Macrander, W. Elam, T. Tyson and Q. Qian, *Rev. Sci. Instrum.*, 2006, **77**, 63901.
34 H. Sternemann, J. Soininen, C. Sternemann, K. Hämäläinen and M. Tolan, *Phys. Rev. B: Condens. Matter Mater. Phys.*, 2007, **75**, 075118.
35 S. K. Lee, J.-F. Lin, Y. Q. Cai, N. Hiraoka, P. J. Eng, T. Okuchi, H.-k. Mao, Y. Meng, M. Y. Hu and P. Chow, *et al.*, *Proc. Natl. Acad. Sci. U. S. A.*, 2008, **105**, 7925–7929.
36 C. J. Sahle, C. Sternemann, C. Schmidt, S. Lehtola, S. Jahn, L. Simonelli, S. Huotari, M. Hakala, T. Pylkkänen and A. Nyrow, *et al.*, *Proc. Natl. Acad. Sci. U. S. A.*, 2013, **110**, 6301–6306.
37 J. Inkinen, A. Sakko, K. Ruotsalainen, T. Pylkkänen, J. Niskanen, S. Galambosi, M. Hakala, G. Monaco, S. Huotari and K. Hämäläinen, *Phys. Chem. Chem. Phys.*, 2013, **15**, 9231–9238.
38 P. S. Miedema, P. Ngene, A. M. van der Eerden, T.-C. Weng, D. Nordlund, D. Sokaras, R. Alonso-Mori, A. Juhin, P. E. de Jongh and F. M. de Groot, *Phys. Chem. Chem. Phys.*, 2012, **14**, 5581–5587.
39 P. S. Miedema, P. Ngene, A. M. Van Der Eerden, D. Sokaras, T.-C. Weng, D. Nordlund, Y. S. Au and F. M. De Groot, *Phys. Chem. Chem. Phys.*, 2014, **16**, 22651–22658.
40 A. Remhof, Y. Yan, D. Rentsch, A. Borgschulte, C. M. Jensen and A. Züttel, *J. Mater. Chem. A*, 2014, **2**, 7244–7249.
41 P. Mauron, M. Bielmann, A. Remhof and A. Züttel, *Rev. Sci. Instrum.*, 2011, **82**, 065108.
42 H. Sternemann, C. Sternemann, G. Seidler, T. Fister, A. Sakko and M. Tolan, *J. Synchrotron Radiat.*, 2008, **15**, 162–169.
43 C. J. Sahle, A. Mirone, J. Niskanen, J. Inkinen, M. Krisch and S. Huotari, *J. Synchrotron Radiat.*, 2015, **22**, 400–409.
44 S. Huotari, T. Pylkkänen, R. Verbeni, G. Monaco and K. Hämäläinen, *Nat. Mater.*, 2011, **10**, 489–493.
45 Y. Filinchuk, R. Cerny and H. Hagemann, *Chem. Mater.*, 2009, **21**, 925–933.
46 Y. Filinchuk, B. Richter, T. R. Jensen, V. Dmitriev, D. Chernyshov and H. Hagemann, *Angew. Chem., Int. Ed.*, 2011, **50**, 11162–11166.
47 V. Ozolins, E. Majzoub and C. Wolverton, *J. Am. Chem. Soc.*, 2008, **131**, 230–237.
48 Y. Zhang, E. Majzoub, V. Ozoliņš and C. Wolverton, *J. Phys. Chem. C*, 2012, **116**, 10522–10528.